Surface & Coatings Technology 324 (2017) 153–166

Contents lists available at ScienceDirect

Surface & Coatings Technology

journal homepage: www.elsevier.com/locate/surfcoat

A first insight on the bio-functionalization mechanisms of TiO_2 nanotubes with calcium, phosphorous and zinc by reverse polarization anodization

Sofia A. Alves [a,b], André L. Rossi [c], Ana R. Ribeiro [b,d,e], Jacques Werckmann [b,f], Jean-Pierre Celis [g], Luís A. Rocha [a,b,h,*], Tolou Shokuhfar [i,j,*]

[a] CMEMS – Center of MicroElectroMechanical Systems, Department of Mechanical Engineering, University of Minho, Azurém, 4800-058 Guimarães, Portugal
[b] IBTN/BR – Brazilian Branch of the Institute of Biomaterials, Tribocorrosion and Nanomedicine, Faculty of Sciences, UNESP – Universidade Estadual Paulista, 17033-360 Bauru, SP, Brazil
[c] Brazilian Center for Research in Physics, 22290-180 Rio de Janeiro, Brazil
[d] Directory of Life Sciences Applied Metrology, National Institute of Metrology, Quality and Technology, 25250-020 Duque de Caxias, RJ, Brazil
[e] Postgraduate Program in Translational Biomedicine, University of Grande Rio, 25070-000 Duque de Caxias, RJ, Brazil
[f] Institute of Biomedical Sciences, UFRJ – Federal University of Rio de Janeiro, 21941-901 Rio de Janeiro, Brazil
[g] Department of Materials Engineering, KU Leuven, 3001 Leuven, Belgium
[h] Faculdade de Ciências, Departamento de Física, UNESP – Universidade Estadual Paulista, 17033-360 Bauru, SP, Brazil
[i] Department of Bioengineering, University of Illinois at Chicago, 60607 Chicago, IL, USA
[j] IBTN/US – American Branch of the Institute of Biomaterials, Tribocorrosion and Nanomedicine, University of Illinois at Chicago, 60612 Chicago, IL, USA

ARTICLE INFO

Article history:
Received 3 March 2017
Revised 18 May 2017
Accepted in revised form 25 May 2017
Available online 26 May 2017

Keywords:
TiO_2 nanotubes
Interface
Reverse polarization
Anodization
Osseointegrated implants

ABSTRACT

The decoration of titanium (Ti) implant surfaces with TiO_2 nanotubes has emerged as a promising strategy to improve osseointegration and avoid infection. Nevertheless, it has been reported that nanotubular films are prone to peeling off from the Ti substrate due to the poor interfacial adhesion. The knowledge on the interfacial properties of such interface, although not well explored, is crucial for understanding the mechanisms behind the poor adhesion problem of these films and to further achieve an easy and effective solution to solve it.

This paper is focused on the bio-functionalization of TiO_2 nanotubular films with zinc (Zn) as an antimicrobial and bone healing agent, together with two major components of bone matrix, namely calcium (Ca) and phosphorous (P). The main aim is, for the first time, the thorough characterization of the interface between TiO_2 nanotubes and the Ti substrate, along with the better understanding of the bio-functionalization mechanisms of TiO_2 nanotubes and their influence on the interfacial features of the films.

TiO_2 nanotubes were successfully synthesized by two-step anodization and their bio-functionalization with Ca, P and Zn was achieved by reverse polarization anodization treatments. The in-depth characterization of the morphological and chemical features of TiO_2 nanotubes was carried out along their length by scanning transmission electron microscopy (STEM) and energy dispersive X-ray spectroscopy (EDS), before and after bio-functionalization treatments. STEM images showed that the interface between conventional TiO_2 nanotubes and Ti is non-continuous due to the existence of a hollow space. However, bio-functionalized TiO_2 nanotubes evidenced an interface with different features, due to the formation of an interfacial oxide film as a consequence of anodization, with a thickness comprised between 230 and 250 nm.

The results presented in this work may inspire the emergence of novel surface treatment strategies seeking the long-term performance of metallic-modified osseointegrated implants.

1. Introduction

Dental implants require the use of materials that are beyond fulfilling requirements such as mechanical, chemical and physical properties, must provide excellent biocompatibility and avoid foreign body responses [1,2]. Along with the discovery of Ti implants, introduced by Brånemark in 1964, revealing the ability of titanium (Ti) to induce osseointegration, the exploration of this material for use in dentistry and orthopedic fields has undergone a global boom [1]. In fact, nowadays, Ti-based materials represent the most widely used in dental and orthopedic fields, owing to their good mechanical properties, excellent biocompatibility and high corrosion resistance, resulting from the spontaneous formation of a thin (of 3–10 nm in thickness) and stable titanium dioxide (TiO_2) film on its surface [1,3,4].

In spite of the high success rate that Ti-based dental implant therapies have reached to replace tooth loss due to trauma or periodontal diseases, a significant number of failures have still been reported to be

* Corresponding author.
E-mail addresses: lrocha@fc.unesp.br (L.A. Rocha), tolou@uic.edu (T. Shokuhfar).

http://dx.doi.org/10.1016/j.surfcoat.2017.05.073
0257-8972/

comprised between 1 and 20% [3,5,6]. Dental implant failures are generally ascribed both to biological (e.g. bacterial infection and inadequate implant-to-bone contact) and biomechanical factors (e.g. occlusal overloading leading to fracture and/or damage of dental implant material) [5,7]. Despite the good biocompatibility of Ti, insufficient osteogenic activity and the lack of antimicrobial properties are the main factors leading to delayed osseointegration and complicated bacterial infections, which may conduce to implant failures, essentially in patients with complex pathologies [4,8–11]. Aiming to overcome the current bone-loss and infection related complications, several studies have been devoted to functionalization of Ti implant surfaces by modifying their features regarding morphology, topography and chemistry [12–15].

Nanotechnology has emerged in the last years as an exciting and successful way to engineer Ti surfaces with nanoscale features for fast integration with bone that is also considered a nanostructured composite matrix [16–19]. Studies have shown that the decoration of Ti-based materials with TiO_2 nanotubes through electrochemical anodization, is a simple and effective way to promote cellular functions, which may be ascribed to their unique morphological, physical and chemical properties [20–23]. The benefits of bio-functionalization of conventional TiO_2 nanotubes have been demonstrated through in vitro and in vivo studies, as they have led to an enhancement on osteoblastic cell functions [24–28], ability to impair bacterial adhesion [29–32] or even both, simultaneously [33,34]. Apart the outstanding properties that bio-functionalized TiO_2 nanotubes have revealed for osseointegrated implants applications [35,36], it has been reported that these films are prone to peeling off from the Ti substrate due to the poor interfacial adhesion between them [37]. This might have catastrophic consequences since, during and after implantation, osseointegrated implants are exposed to tribological and tribocorrosive conditions, which may induce to film degradation accompanied by the release of wear debris and corrosion products to implant surroundings, triggering harmful biological effects and ending up in implant failure [38–45].

A few studies have been reported seeking to understand the poor adhesion of TiO_2 nanotubes to Ti substrate. In accordance with Miraghaei et al. [46] TiO_2 nanotubes detach easily from the substrate due to the dissolution of a fluoride-rich layer existing between the tubes and Ti. Moreover, a hydrogen-assisted crack mechanism induced by the existence of Ti—H and hydrogen blisters in the bottom layer of the nanotubes was proposed by Zhao et al. [47]. The beneficial effect of anodization of TiO_2 nanotubes on their adhesion strength to Ti was reported by Yu et al. [37], which was ascribed to the formation of a compact layer near the nanotube bottom. However, the characteristics of Ti/TiO_2 film interface before and after anodization, were not reported. The knowledge of the characteristics of Ti/TiO_2 nanotubes interface is still very limited in literature, which is an issue of crucial importance to well-understand the poor adhesion problem of these films and to further achieve an effective solution to solve it. A new methodology for TiO_2 nanotubes bio-functionalization through reverse polarization anodization was described by our group in previous works [48,49]. After bio-functionalization treatments, biocompatible TiO_2 nanotubes were synthesized displaying superior corrosion behavior than conventional nanotubes [48]. Additionally, the tribo-electrochemical behavior of TiO_2 nanotubes was significantly improved after bio-functionalization treatments, which was correlated with their improved adhesion strength to the Ti substrate, granted by the formation of a film at the interface region [49]. The focus of the present contribution is on the bio-functionalization of the TiO_2 nanotubes with Ca, P and Zn by reverse polarization anodization. The main aim relies, for the first time, on the in-depth morphological and chemical characterization of the TiO_2 nanotubes along their length, with special focus at the interface region, before and after bio-functionalization treatments. A first insight on the bio-functionalization mechanisms of TiO_2 nanotubes by reverse polarization and anodization processes is presented.

2. Materials and methods

2.1. Surface pre-treatment

Commercially pure titanium (cp-Ti grade 2) (American Society for Testing of Materials – Grade 2) (MacMaster-carr, IL, USA) rods cut into discs of 15 mm diameter and 2 mm thickness were the substrates used in this study. A series of silicon carbide (SiC) sandpapers #240, #320, #400, #600 and #800 were used to ground cp-Ti surfaces followed by their polishing with alumina suspension untill achieve a mirror finishing. After polishing, the Ti samples were ultrasonically cleaned in ethanol (10 min) and distilled (DI) water (5 min), followed by drying at room temperature.

2.2. Synthesis of TiO_2 nanotubes by two-step anodization

Titanium dioxide (TiO_2) nanotubes were synthesized by two-step anodization of Ti in an optimized electrolyte constituted of ethylene glycol (EG), 0.3 wt% ammonium fluoride (NH_4F) (VETEC, Xerém, Rio de Janeiro, Brazil) and 3 vol% DI water. The electrolyte was continuously stirred (150 rpm) at room temperature (22 to 24 °C). The anodic treatments were conducted using a dc power supply (KEYSIGHT, N5751A) with a limiting current of 2.5 A.

Firstly, Ti polished samples (anode, surface area: 4.5 cm^2) and a graphite rod (cathode, surface area: 1.5 cm^2) were almost completely immersed in the EG-based electrolyte, and only a small area was not in contact with the solution, i.e., the correspondent place where the metallic alligator clip was holding the electrodes. To control the reproducibility of the anodic film features, one must be highlighted that the side of the Ti sample intended to be treated and considered for further characterization studies was always facing the graphite rod, and these two electrodes were placed parallel to each other separated at a fixed distance of 2 cm. The electrochemical treatments were conducted at 60 V for 1 h.

The resulting nanotubes grown from Ti through this first anodization step, were intentionally removed by ultrasonication in isopropanol for 15 min followed by cleaning in DI water for 5 min. Secondly, the resulting nanopatterned Ti surfaces were anodized at the previous conditions for 30 min. The second anodization step resulted in the growth of self-ordered TiO_2 nanotube arrays, which were named as NT. Immediately after the second anodization step, NT samples were rinsed with DI water and dried at room temperature.

2.3. Bio-functionalization of TiO_2 nanotubes with calcium, phosphorous and zinc by reverse polarization and anodization

The TiO_2 nanotubular samples were bio-functionalized by reverse polarization and anodization processes, aiming the doping of nanotubes with calcium (Ca), phosphorous (P) and zinc (Zn) elements. Cathodic and anodic treatments were performed in an aqueous electrolyte constituted of calcium acetate (CaA) (Calcium acetate monohydrate, VETEC, Xerém, Rio de Janeiro, Brazil) and β-glycerolphosphate (β-GP) (β-glycerolphosphate disodium salt pentahydrate, Sigma-Aldrich, St. Louis, MO, USA) as the source of Ca and P, respectively, and this electrolyte was named as Ca/P-based electrolyte (pH = 7.92 ± 0.06). The concentrations of CaA (0.35 M) and β-GP (0.04 M) in the electrolyte were established in accordance with the experimental procedures followed in previous works [48,50–52], with Ca/P ratio of 19.75. Zinc acetate (Zinc acetate dihydrate, Sigma-Aldrich, St. Louis, MO, USA) at a concentration of 0.35 M was added to the previous Ca/P-based electrolyte aiming the additional incorporation of Zn in the nanotubular structure, and this solution was named as Ca/P/Zn-based electrolyte (pH = 6.52 ± 0.01).

The reverse polarization and anodization treatments were conducted using a dc power supply (KEYSIGHT, N5751A) set with a limiting current of 2.5 A. For reverse polarization step, the NT samples were set as

the cathode (surface area: 4.5 cm^2) and a graphite rod as the anode (surface area: 1.5 cm^2), and these were immersed in the Ca/P-based electrolyte, at the previously described configuration in section 2.2. The power suply was set at 20 V for 30 s. After 1 min, the electrodes polarity was inverted, and the anodization step was carried out in the same electrolyte for 30 min at 100 V. These samples were named as NT-Ca/P. Additionally, NT samples were treated in the Ca/P/Zn-based electrolyte, at the previous reverse polarization and anodization conditions, and were named as NT-Ca/P/Zn. All the reverse polarization and anodization treatments were carried out under magnetic stirring at 200 rpm.

2.4. Characterization of TiO_2 nanotubular films

TiO_2 nanotubular samples before and after bio-functionalization treatments were mounted on a stub with double sided conductive carbon tape, and their morphology was analyzed by scanning electron microscopy (SEM) using a FEI Helios NanoLab 650. This instrument was equipped with a detector for energy dispersive X-ray spectroscopy (EDS). EDS spectra and elemental maps were acquired to evaluate the chemical composition of the nanotubular samples and the distribution of the elements.

For a better understanding of the bio-functionalization mechanisms of TiO_2 nanotubes, the morphological and chemical features of the nanotubes were evaluated along their length. For this purpose, thin cross-sections of the nanotubular films (around 100 nm thick) were obtained in a dual beam instrument equipped with focused ion beam (FIB) (TESCAN LYRA 3) operated with gallium (Ga) ion source. A thin gold (Au) layer was previously deposited to the film surface to improve the electrical conductivity. A platinum (Pt) layer of 1 μm was locally deposited in situ using a gas injection system and 1 nA Ga^+ ion current accelerated at 30 keV. Initial etching was performed with 5 and 2 nA at 30 keV. The lamella was then transferred to a copper (Cu) transmission electron microscopy (TEM) grid using a nanomanipulator and Pt deposition. Thinning was performed in 3 steps to obtain a lamella of ~100 nm: 1) 1 nA/30 keV; 2) 0.1 nA/10 keV; 3) 10 pA/5 keV. A final step was accomplished with ~5 pA/3 keV to reduce the damaged layer produced during the thinning process.

FIB cross-sections were investigated by TEM and dark-field scanning transmission electron microscopy (STEM-DF) using a JEOL 2100F operating at an accelerating voltage of 200 kV. EDS spectra and elemental maps were obtained in the same instrument with an EDS detector (Noran Seven), in STEM mode (STEM-EDS). Selected area electron diffraction patterns were obtained to investigate the crystallinity of the anodic oxide films.

3. Results

3.1. Surface characterization

Well-defined and well-organized TiO_2 nanotube arrays were fabricated by two-step anodization in a fluoride (F^-) containing electrolyte, whose surface morphology is depicted in Fig. 1a. These samples are mainly composed of Carbon (C), Ti, Oxygen (O) and Fluorine (F) as observed in the correspondent EDS spectrum in Fig. 1b. As demonstrated by XPS studies carried out in a previous work [48], NT surfaces are composed of Ti and O mainly as TiO_2.

TiO_2 nanotubular samples were submitted to cathodic and anodic treatments aiming their functionalization with bioactive elements, namely calcium (Ca), phosphorous (P) and zinc (Zn). For this purpose, NT samples were reverse polarized in a Ca/P-based electrolyte and, immediately after, anodized in the same solution. The surface morphology of NT-Ca/P samples is shown in Fig. 1c, and the correspondent EDS spectrum shows the presence of Ca and P elements (Fig. 1d). To achieve the incorporation of Zn, together with Ca and P, NT samples were submitted to reverse polarization and anodization processes in a Ca/P/Zn-based electrolyte, and the morphology of the fabricated nanotubes is shown in Fig. 1e. The presence of Zn is confirmed by the EDS spectrum shown in Fig. 1f. No significant differences are observed on the nanotube surface morphology before and after bio-functionalization treatments.

The EDS elemental maps in Fig. 2a show the homogeneous distribution of Ti, O and F along the surface of NT samples. Similar results were obtained for the elemental distribution of these elements on NT-Ca/P and NT-Ca/P/Zn samples (results not shown). The elemental maps of Ca and P extracted from NT-Ca/P samples are shown in Fig. 2b, while

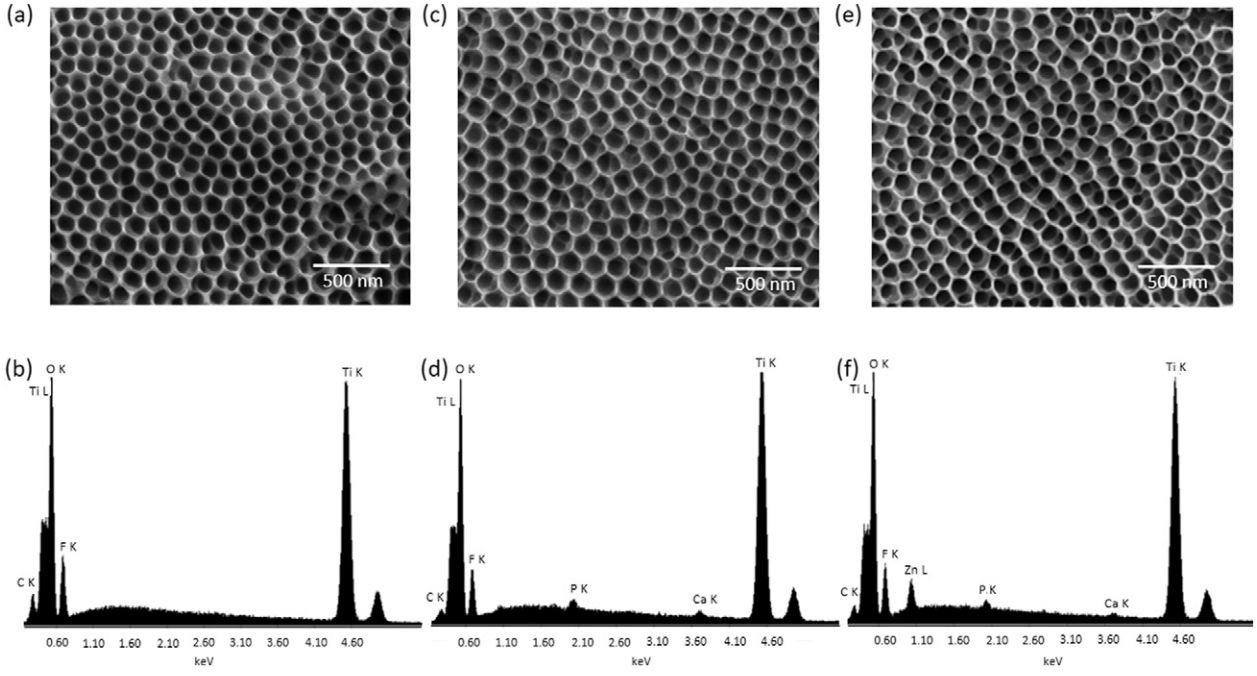

Fig. 1. SEM micrographs and EDS spectra showing the surface morphology and elemental composition of (a) and (b) NT; (c) and (d) NT-Ca/P; (e) and (f) NT-Ca/P/Zn samples.

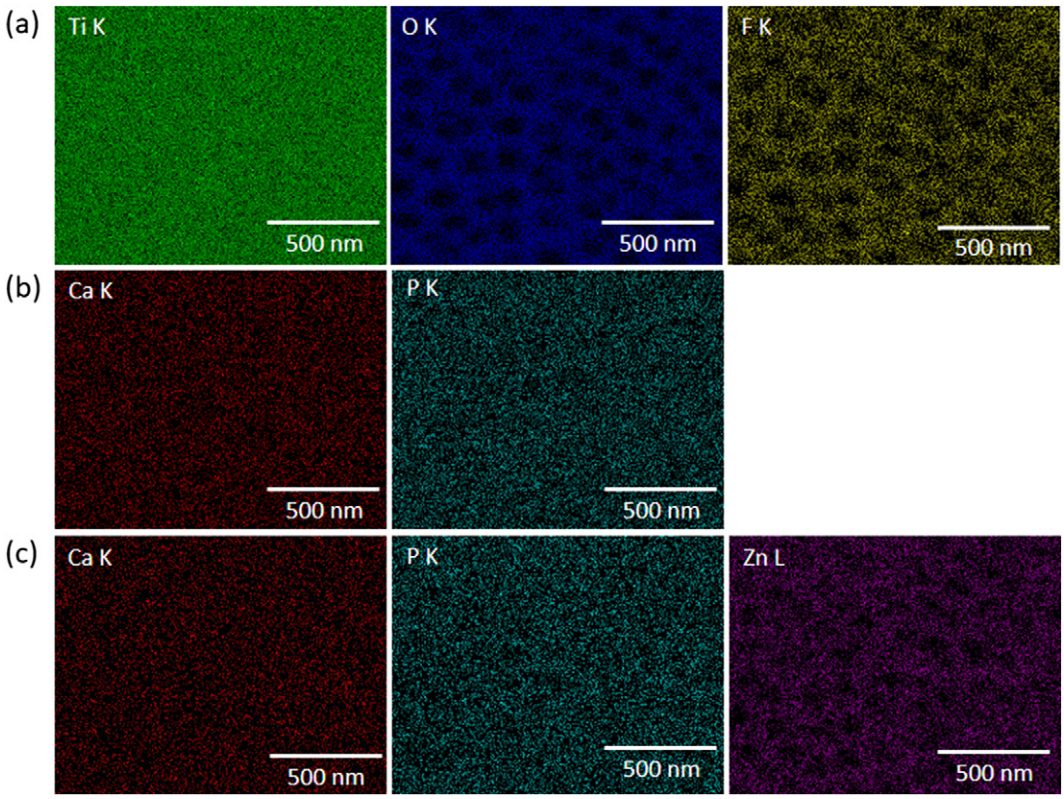

Fig. 2. (a) Elemental maps representative of Ti K, O K and F K extracted from NT samples. In (b) the elemental maps of Ca K and P K obtained from NT-Ca/P samples are depicted, while in (c) are presented the maps for Ca K, P K and Zn L elements acquired from NT-Ca/P/Zn samples. The elemental maps were obtained from the samples shown in Fig. 1.

in Fig. 2c the elemental distribution of Ca, P and Zn on NT-Ca/P/Zn samples is depicted.

3.2. Cross-sectional characterization of nanotubular films

Thin cross-sectional slices of the nanotubular films with approximately 100 nm thickness were obtained by FIB, then imaged by TEM and STEM and analyzed by EDS. The general overview of TiO_2 nanotubes produced by two-step anodization is depicted in Fig. 3a. From this TEM image the thickness of the film was measured as 6.1 ± 0.1 μm. In Fig. 3b a higher magnification STEM-DF image representative of the cross-sectional view of TiO_2 nanotubes in the top region of the film is shown. The region from which the magnified image was taken is indicated by the inset square in Fig. 3a named as A1. From this image the wall and the hollow part of the nanotubes can be observed and, in general, the tubes are well aligned and present a uniform morphology. Furthermore, the insertion in this image shows the electron diffraction pattern composed of diffuse rings indicating an amorphous nature of TiO_2 nanotubes for this region of the film. To study the elemental distribution along the nanotubular films thickness, STEM-EDS elemental maps of Ti, O and F were acquired in the upper part and at the interface region. As observed from elemental maps depicted in Fig. 3c – A1, representative of the upper part of TiO_2 nanotubular films, it is observed that Ti, O and F are uniformly distributed along the nanotube thickness. Similar features are observed at the interface region shown in Fig. 3c – A2, where the distribution of these elements is also uniform. The interface between TiO_2 nanotubes and Ti can be easily identified in the maps by the lower O and F colour intensity in the area related to Ti substrate and, on the contrary, by the higher intensity of the colour for Ti in this region.

The morphological and chemical features of TiO_2 nanotubes were also investigated after bio-functionalization treatments with Ca and P. The TEM image representative of the FIB cross- section of NT-Ca/P film is shown in Fig. 4a. The nanotube length, i.e. the thickness of the film, was measured as 4.8 ± 0.1 μm. The upper part of the film was imaged at higher magnification as shown in Fig. 4b, in which well-aligned single nanotubes are clearly observed. The STEM-EDS spectrum obtained from the region indicated by the inset red square A in Fig. 4b, is shown in Fig. 4c. From this spectrum it is observed that C, Ti, O, F and Ca were detected in the superficial region of the film (until approximately 1 μm depth). Additional chemical elements such as Cu, Ga, Silicon (Si), Au and Pt were also detected in the uppermost regions of NT-Ca/P (Fig. 4c) film. The presence of Cu is related to the Cu grid used for TEM and STEM analyses, while the Ga is related to the Ga primary ion beam used by FIB system. Additionally, the detection of a small signal of Si is probably related with the internal fluorescence peak from Si dead layer of Si—Li detector [53]. Finally, the presence of Au and Pt are related to the Au surface coating performed before sample preparation by FIB, and to the Pt protection against Ga ions during polishing. The inset spectrum in Fig. 4c, with energy values comprised between 2 and 5 keV, intends to show in more detail the peak of Ca. In this spectrum, the escape peak for Ti K (Ti K - Si K = 2.77 keV) is also observed. After bio-functionalization processes in the Ca/P/Zn-based electrolyte, nanotubular films with a length of 4.6 ± 0.1 μm were produced, as shown in Fig. 5a. The STEM-DF image of the uppermost region of NT-Ca/P/Zn film is shown in Fig. 5b, from which well-ordered and single nanotubes are observed. Bright dots are Pt and Au particles that penetrated the TiO_2 nanotubes during samples preparation for FIB sectioning. The STEM-EDS spectrum acquired from the area highlighted by the inset red square in Fig. 5b is depicted in Fig. 5c. From this spectrum, elements such as C, Ti, O and F were identified, including Ca and Zn as shown by the more detailed spectrum added in the figure, with energy values comprised between 3 and 10 keV. Once again, the presence of elements such as Cu, Ga, Si, Au and Pt were detected, whose source was previously explained in the above description of Fig. 4c. Additionally, Chromium (Cr), Iron (Fe) and Cobalt (Co) were also present in the upper part of these films, which are most likely related to contamination from the metallic alligator clip used as the electrical conductive holder of Ti samples

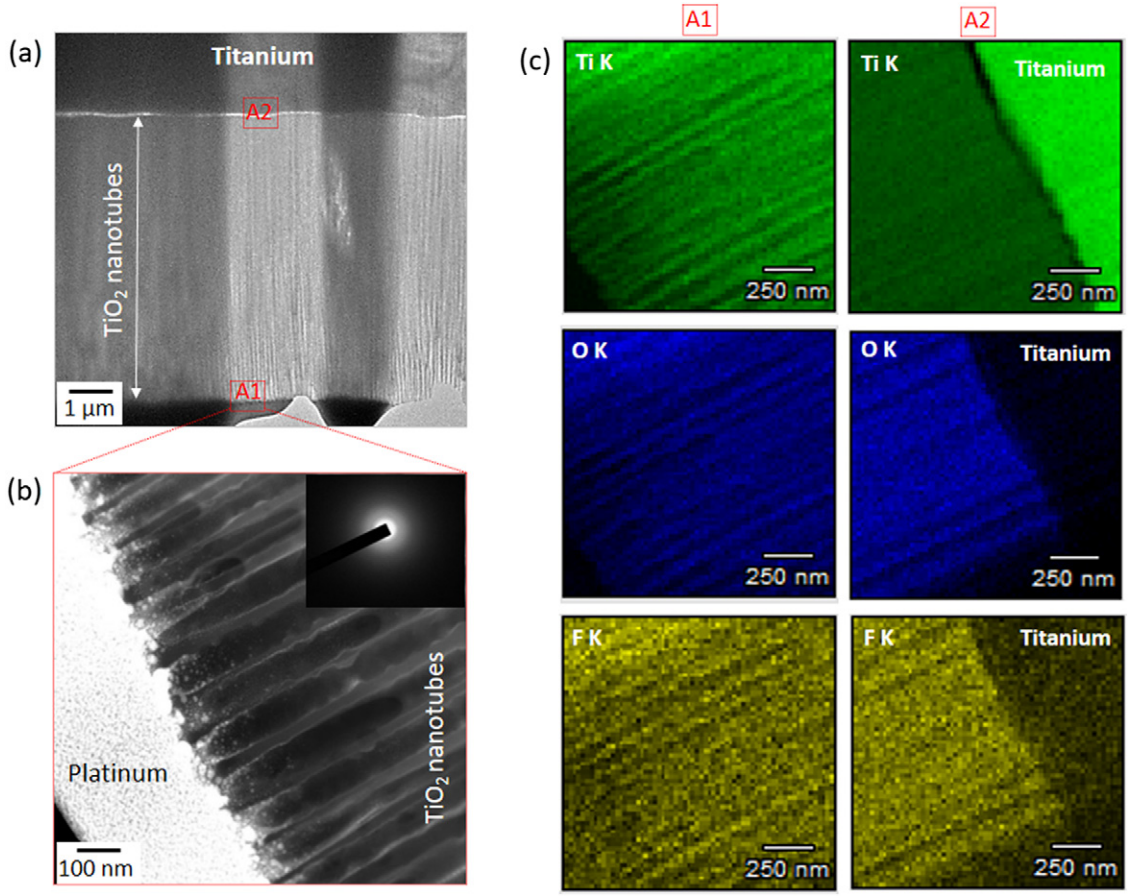

Fig. 3. TEM and STEM-DF images of the FIB cross-section of TiO_2 nanotubular film synthesized by two-step anodization: (a) general overview of the film; (b) upper region of the film. The inset in (b) shows the electron diffraction pattern obtained for TiO_2 film. In (c) are shown the STEM-EDS elemental maps of Ti K, O K and F K obtained from two different regions in the TiO_2 nanotubular film shown in (a): A1 – the upper region of the film; A2 – the region at the Ti/film interface.

during anodization processes. It is noteworthy to highlight that additional contributions were found for both films at the elemental energy of P, which are related to Pt and Au. Therefore, it is not possible to accurately identify this element in both spectra (Fig. 4c and Fig. 5c). However, from the EDS surface spectra obtained from NT-Ca/P (Fig. 1d) and NT-Ca/P/Zn (Fig. 1f) samples (prepared without Au and Pt), it is expected that P compounds are present in this region of the films.

For a better understanding on the elemental distribution along the length of the nanotubes in the top region of the films, STEM-EDS spectra were acquired from different regions along the STEM images depicted in Fig. 4b and Fig. 5b (Supplementary material). From these results, the elements were found uniformly distributed along the nanotube length, and no gradient on their atomic concentration was observed. Similar results were found for STEM-EDS analysis carried out in the central part of the bio-functionalized nanotubular films (Supplementary material).

Aiming to study the interfacial features of TiO_2 nanotubular films, before and after bio-functionalization processes, STEM-DF images were taken at the interface regions. The lower and higher magnification STEM-DF images at the interface of TiO_2 nanotubular films are shown in Fig. 6. The region of Ti substrate is easily identified as the brighter area contrasting with the darker region related to TiO_2 nanotubes, as indicated in the image. A non-continuous interface is observed between TiO_2 nanotubes and the Ti substrate, as shown by the darker region appearing between TiO_2 nanotubes and Ti. This interface is characterized by a hollow space as indicated by the inset white arrow in Fig. 6b, and is found along the extension of the film with a thickness at a nanoscale range (35 ± 4.3 nm).

After bio-functionalization treatments, remarkable changes were observed at the interface, as the hollow space became partially filled, with some defects still present. The interface regions of NT-Ca/P and NT-Ca/P/Zn films are shown in Fig. 7a and b, respectively, with both films presenting an interface with similar morphological features. From higher magnification STEM-DF images shown in Fig. 7c and d, it is observed a porous interface characterized by the presence of an oxide film between, below and above the pores. A second interface was found in these films, as observed from the lines appearing along the films length, which are indicated by the inset white arrows in the figures. This second interface delimitates the thickness of newly-formed oxide films, whose values are comprised between 230 and 250 nm for both nanotubular films. NT-Ca/P and NT-Ca/P/Zn films are overall amorphous, as confirmed from electron diffraction patterns obtained from the lower, middle and upper regions of the films, characterized by broad and diffuse rings in every case (results not shown).

For a better knowledge of the differences observed at the interface region before and after bio-functionalization treatments, the current vs. time curves were recorded during all the anodization processes (Fig. 8). The current vs. time evolution recorded during the second step of anodization for TiO_2 nanotube formation is shown in Fig. 8a. This is a typical curve showing the three main stages of current achieved during anodization of Ti for nanotube formation [54]. Firstly, there is a decrease in the current values from 60 mA (13.3 mA/cm^2) until approximately 15 mA (3.3 mA/cm^2). Afterwards, a slight increase in the current is observed until 20 mA (4.4 mA/cm^2) followed by a period of stabilization until the end of the anodization process. The current evolution achieved during bio-functionalization of NT samples in the Ca/P-based electrolyte is observed in Fig. 8b. In this curve it is shown the initial period of reverse polarization applied for 30 s, in which the current values were kept approximately at 750 mA (166.7 mA/cm^2). In the inset graph

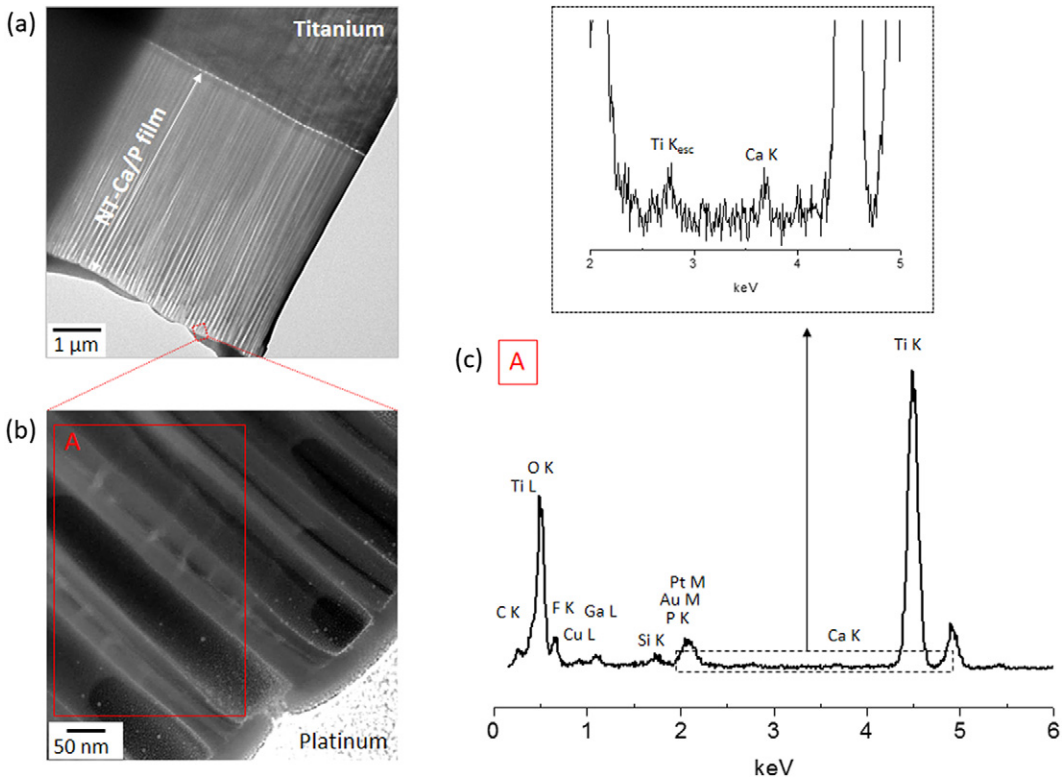

Fig. 4. TEM and STEM-DF images of the FIB cross-section of NT-Ca/P film: (a) TEM image showing a general overview of the film; (b) upper region of the film. In (c) the STEM-EDS spectrum obtained from the area correspondent to the inset red square A in (b) is shown. The inset spectrum in (c), with energy values comprised between 2 and 5 keV, intends to show in more detail the detected peak for Ca K.

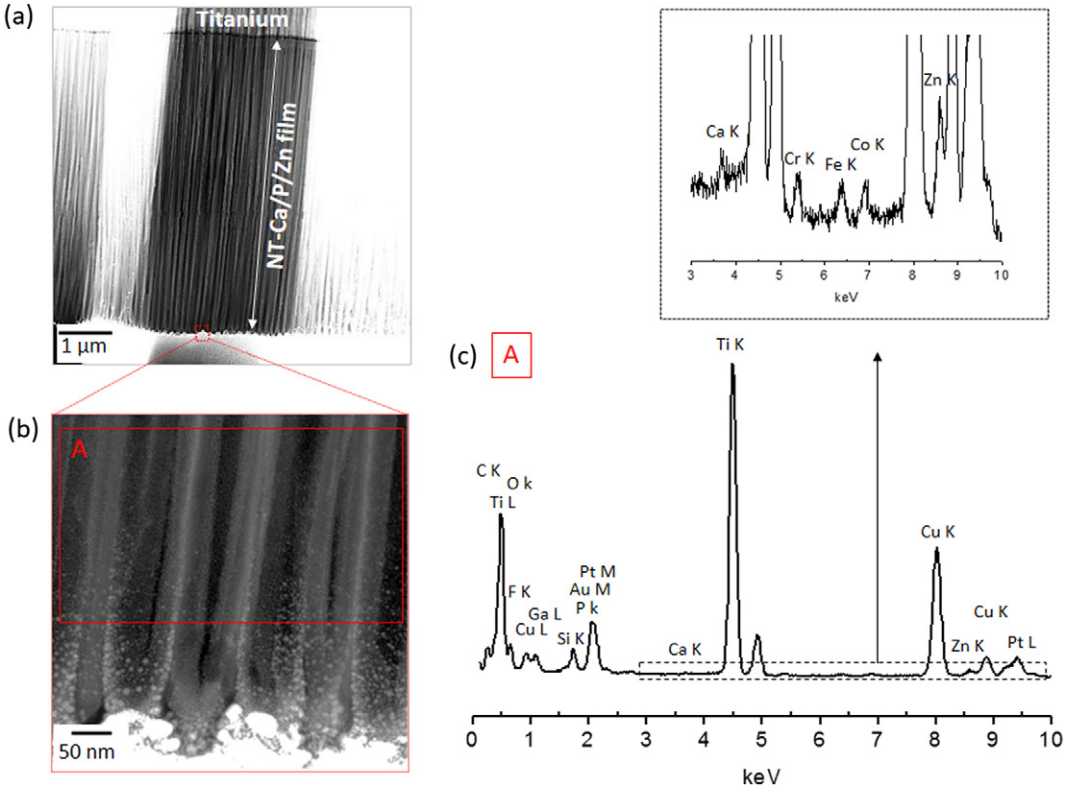

Fig. 5. STEM-DF images of the FIB cross-section of NT-Ca/P/Zn film: (a) general overview of the film; (b) upper region of the film. In (c) the STEM-EDS spectrum obtained from the area correspondent to the inset red square A in (b) is depicted. The inset EDS spectrum in (c), with energy values comprised between 3 and 10 keV, intends to show in more detail the detected peaks for Ca K and Zn K elements.

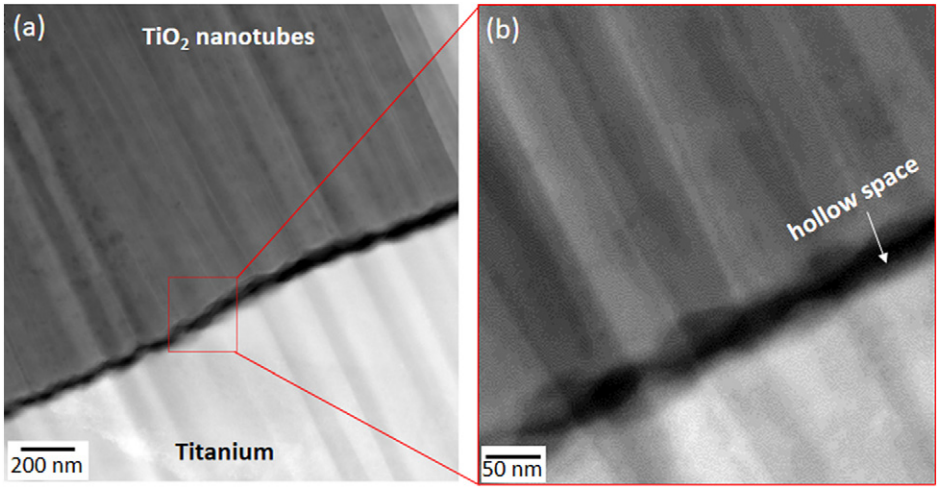

Fig. 6. STEM-DF images of the FIB cross-section of TiO_2 nanotubular films in the interface region at (a) lower and (b) higher magnifications.

in Fig. 8b it is observed the evolution of the current during the anodization step carried out at 100 V for 30 min. As observed, as soon as a voltage of 100 V is applied, the current reaches the limiting value of 2.5 A (0.5 A/cm^2) for a few milliseconds, followed by a sudden decrease until 9.2 mA (2 mA/cm^2), a value that was kept constant until the end of the anodization period. The current vs. time evolution recorded during the synthesis of NT-Ca/P/Zn samples, is shown in Fig. 8c. In this case, during anodization, the current was kept at 2.5 A for a longer period (a few seconds), before it reaches values of 9.2 mA (2 mA/cm^2).

The chemical features of the interface of bio-functionalized films were studied aiming a better comprehension of the relation between the current vs. time evolution recorded during anodization, with their characteristics. For this purpose, line profile STEM-EDS analyses were carried out at the interface of NT-Ca/P films (Fig. 9a). The spectrum in

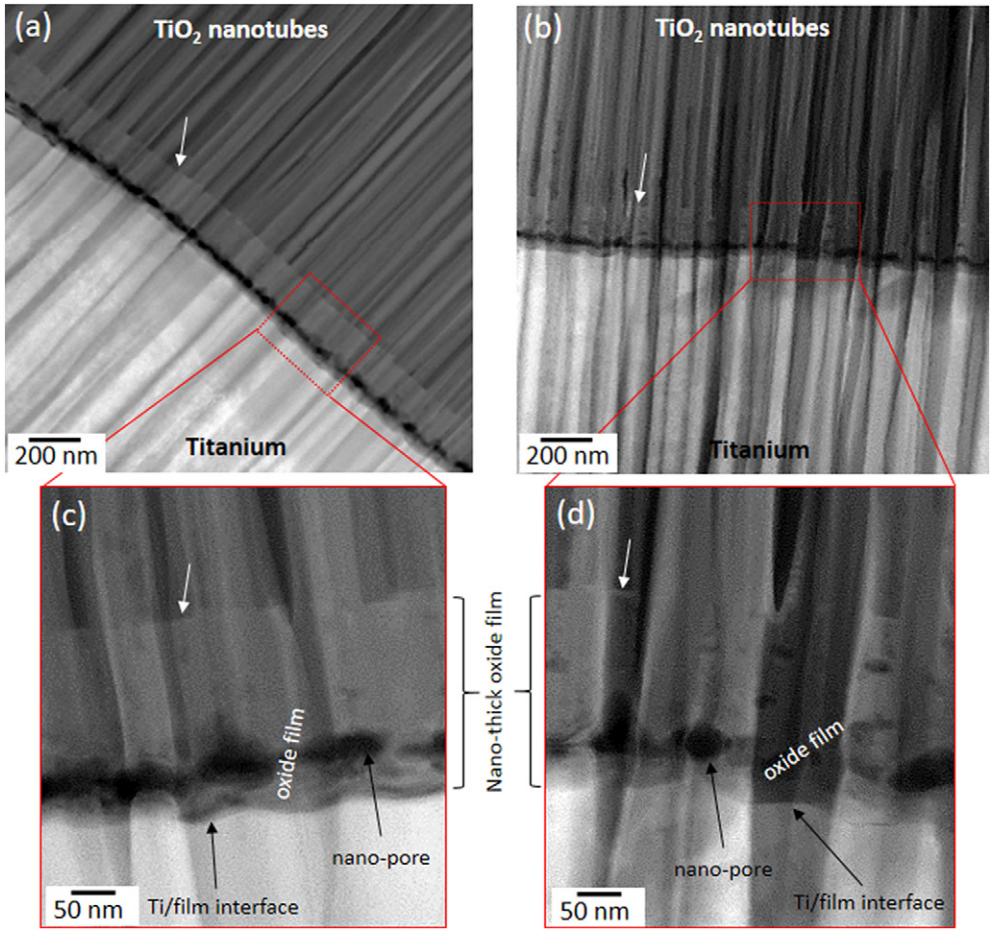

Fig. 7. STEM-DF images of the FIB cross-sections of (a) NT-Ca/P and (b) NT-Ca/P/Zn films in the interface region. Higher magnification images are shown in (c) and (d) for the region highlighted by inset red squares in (a) and (b), respectively. The white arrows show the interface between the nano-thick oxide films (grown during bio-functionalization processes) and TiO_2 nanotubes.

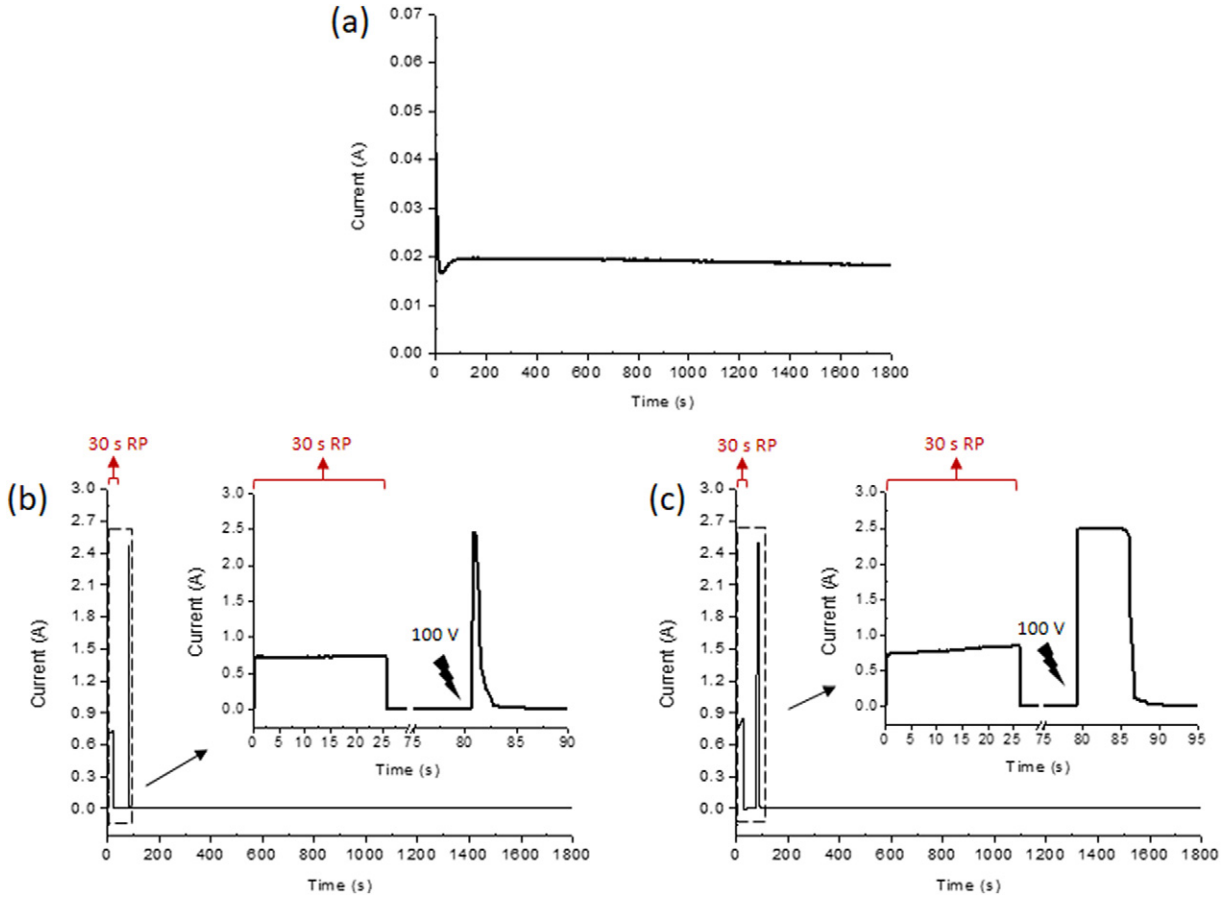

Fig. 8. (a) Current vs. time evolution during the second anodization step of nanotextured Ti for TiO_2 nanotube synthesis. The current evolutions during 30 s of reverse polarization (30 s RP) and 30 min of anodization are shown for treatments carried out in the (b) Ca/P and (c) Ca/P/Zn-based electrolytes. The inset graphs in (b) and (c) intend to show in more detail the current evolution during the initial stage of anodization processes.

Fig. 9b was extracted from the inset white square A in Fig. 9a, and it shows the presence of Ca and P, jointly with other elements such as Ti, O, F, Ga and Si. The STEM-EDS elemental maps showing the distribution of Ti, O and F at the interface region are shown in Supplementary material. The STEM-EDS spectra acquired from line scan analyses performed in three different spots at the interface of NT-Ca/P films is shown in Fig. 9c. These analyses were carried out along the uppermost part of the nano-thick film formed by anodization, as indicated by a, b and c white spots inserted in Fig. 9a. As it is observed, Ti, O and F were found along this line, however, there is a peak of Ca, only detected in point b. To check the Ca distribution outside and inside this interface, additional STEM-EDS analyses were carried along the points 1, 2 and 3 (shown in Fig. 9a), whose spectra are shown in Fig. 9d. The expected elements were found, namely Ti, O and F. Interestingly, the peak for Ca was also found only in point 2, evidencing the entrapment of this element at that place. Finally, the chemical features of the interface of NT-Ca/P/Zn films (Fig. 10a) were investigated. The general spectrum acquired from the area delimited by the inset white square in Fig. 10a is shown in Fig. 10b. The presence of the elements, such as Ti, O, F, Si, P, Ca and Zn was detected. The STEM-EDS elemental maps showing the distribution of Ti, O and F at the interface region of NT-Ca/P/Zn film are shown in Supplementary material. Line scan STEM-EDS analyses were carried out at 7 specific points across the nano-thick oxide film formed by anodization (shown in Fig. 10a), and the correspondent acquired spectra are shown in Fig. 10c. The STEM-EDS analysis for each point, shows clearly the presence of P and Zn elements non-uniformly distributed across the interface. The presence of P appeared more pronounced in the intermediate zone of the film, as shown by the peaks of P found in the spots numbered from 2 to 6. Moreover, the presence of Zn was found more prominent in the spots 3 and 5.

It is noteworthy to highlight that in some of the presented spectra part of the elemental peaks are not being depicted in full, once a more detailed view of the less counted peaks is aimed.

4. Discussion

4.1. Morphological and chemical features of bio-functionalized TiO_2 nanotubes

Multi-step anodization of Ti in a fluoride-containing electrolyte has been extensively employed to synthesize TiO_2 nanotubes with improved self-ordering [18,19,23,28,32,35,36,54–57] .To achieve the desired bone-inspired surface morphology observed in Fig. 1a, TiO_2 nanotubes were synthesized by anodization of a nano-patterned Ti surface with the nanotube bottom hemispherical morphology, resulted from a first anodization step of a Ti smooth surface, in which TiO_2 nanotubes were grown drilling their rounded bottom, and afterwards, intentionally removed [54]. During anodization, it is believed that nanotubes growth is based on electric field assisted oxidation and dissolution processes, which rely on the formation of a passive Ti oxide film through the recombination of Ti^{4+}, O^{2-} and OH^- ions and the local chemical dissolution of the growing oxide by F^- ions [54,58].

NT surface morphology is characterized by the presence of bigger and smaller pores, and in some cases, the formation of multiple pores inside a bigger pore is observed (Fig. 1a). Macak et al. [59] observed that, in the very first stage of TiO_2 nanotube growth, a thin and non-

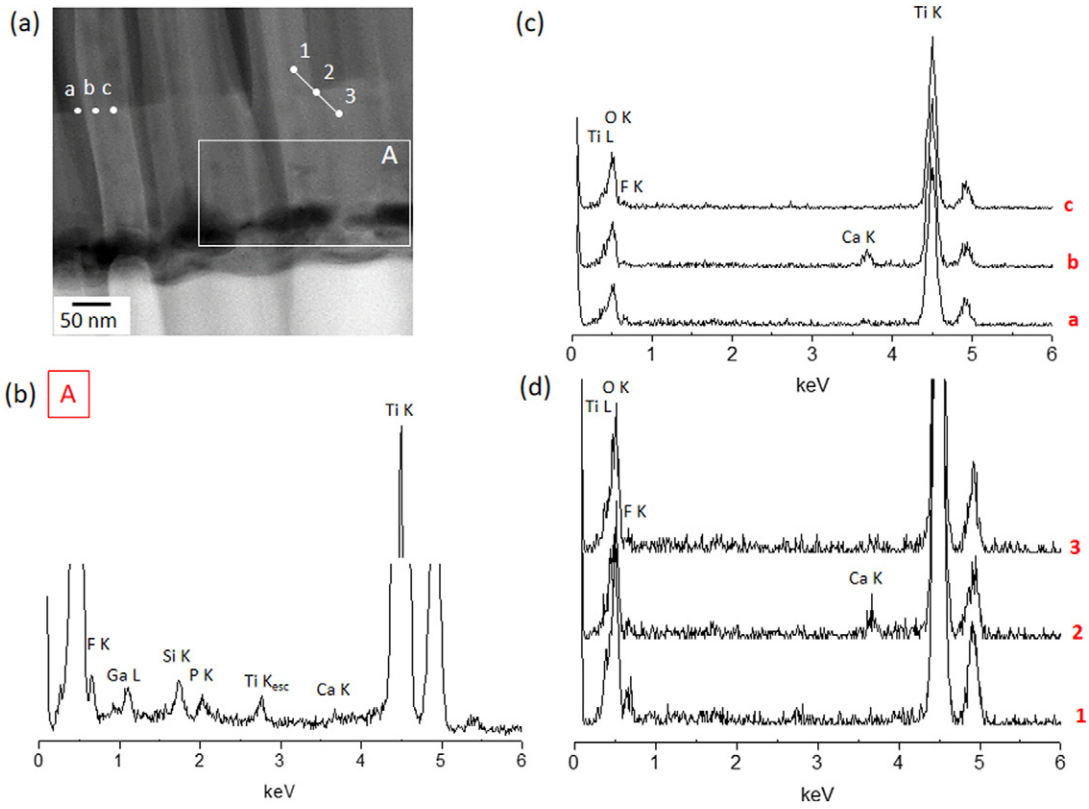

Fig. 9. STEM-EDS analyses in the interface region of NT-Ca/P film: (a) STEM-DF image showing the NT-Ca/P film interface, with the white insets indicating where the elemental analyses were performed; (b) STEM-EDS spectrum obtained from the region comprised in the inset red square A in (a); (c) line scan STEM-EDS analyses along the uppermost part of the nano-thick oxide film formed by anodization, as indicated by a, b and c white spots inserted in (a); (d) line scan STEM-EDS analyses across the uppermost part of the nano-thick oxide film, as indicated by the inset white number 1, 2 and 3 in (a).

porous layer was formed where localized accelerated dissolution occurred under the action of the electric field. From two-step anodization, it is expected that the nano-imprints generated from the first anodizing step act as nucleation sites for initial pore formation and thus, behave as an intentionally designed template to trigger localized dissolution and obtain the desired final morphology [58]. The formation of multiple pores inside a main one is probably related with the events taking place in the beginning of the second anodization step. Possibly, the primary localized dissolution occurred in multiple sites inside the same nano-dimple, resulted from the first anodization step. Macak et al. [59] observed that the surface morphology is maintained after 10 min of anodization. Thus, it is expected that the surface morphology resulting from the primary localized dissolution is preserved over time, since during anodization, pronounced dissolution takes place at the bottom of the pores, where the electric filed is stronger, making them significantly deeper over time [58,59]. The illustration of the different growth stages of TiO_2 nanotubes from nano-patterned Ti substrates is schematically shown in Fig. 11a – c.

The bone-inspired TiO_2 nanotubes were doped with Ca and P, whose morphology and composition are shown in Fig. 1c and d, respectively. Reverse polarization anodization in a Ca/P-based electrolyte appeared as a very promising way to modify the chemistry of the nanotubes without compromising their morphological features. In accordance with our previous study, Ca and P elements are possibly assigned to the presence of $Ca_3(PO_4)_2$/$CaHPO_4$, CaF_2, $CaCO_3$ and CaO species [48]. Beyond bone-constituting Ca and P, TiO_2 nanotubes were also bio-functionalized with Zn, which plays a major role in bone remodeling while exhibiting antibacterial properties [60]. The incorporation of Ca, P and Zn was successfully achieved by reverse polarization anodization of TiO_2 nanotubes in the Ca/P/Zn-based electrolyte (Fig. 1f), with no differences observed on the acquired morphology (Fig. 1e), when compared to NT and NT-Ca/P samples. In general, the bioactive elements (i.e. Ca, P and Zn) are uniformly distributed along the TiO_2 nanotubular samples, as observed in EDS elemental maps shown in Fig. 2b and c.

TiO_2 nanotubes were grown perpendicularly oriented to the Ti substrate (Fig. 3a) with high self-ordering level, as observed through single nanotubes depicted in the STEM-DF image of the upper part of the film (Fig. 3b). STEM-EDS elemental maps taken in the upper part and at the interface region of the film show the presence of Ti, O and F along the nanotubes length (Fig. 3c). Berger et al. [61] proved for the first time that TiO_2 nanotubes grown in fluoride-based ethylene glycol electrolytes form a fluoride rich layer (few nm thick) between the individual nanotubes, and this might be the reason for the detection of fluoride species all over the nanotubular layer through STEM-EDS analysis.

After bio-functionalization of TiO_2 nanotubes in both electrolytes, the high level of ordering and integrity of the tubes is maintained along their length, and single nanotubes are clearly seen without any aggregates along the tube walls (Fig. 4 and Fig.5). As regards the thickness of TiO_2 nanotubes, this was reduced after bio-functionalization treatments. In accordance with our previous work [48], the thinning phenomenon of the film is related with the reverse polarization step, during which the reduction of TiO_2 to $TiO_{2-x}(OH)_x$ (e.g. TiOOH) is expected to take place, followed by its chemical dissolution in the electrolyte [62–65]. Furthermore, one must be considered that the dissolution of the oxide film may also occur right after the period of reverse polarization, i.e. when the anodic polarization step starts. During anodic polarization of TiO_2 nanotubes in the Ca/P and Ca/P/Zn-based electrolytes, a high peak of current is observed in both cases, during which the creation of very acidic conditions inside the tubes is expected to take place and consequently induce to the dissolution of the oxide [66,67]. This may further explain the lower thickness of NT-Ca/P/Zn when compared to NT-Ca/P films, since the pH of the Ca/P/Zn-containing electrolyte is lower and the duration of the high current period is longer for the anodization process carried out in this solution (Fig. 8b

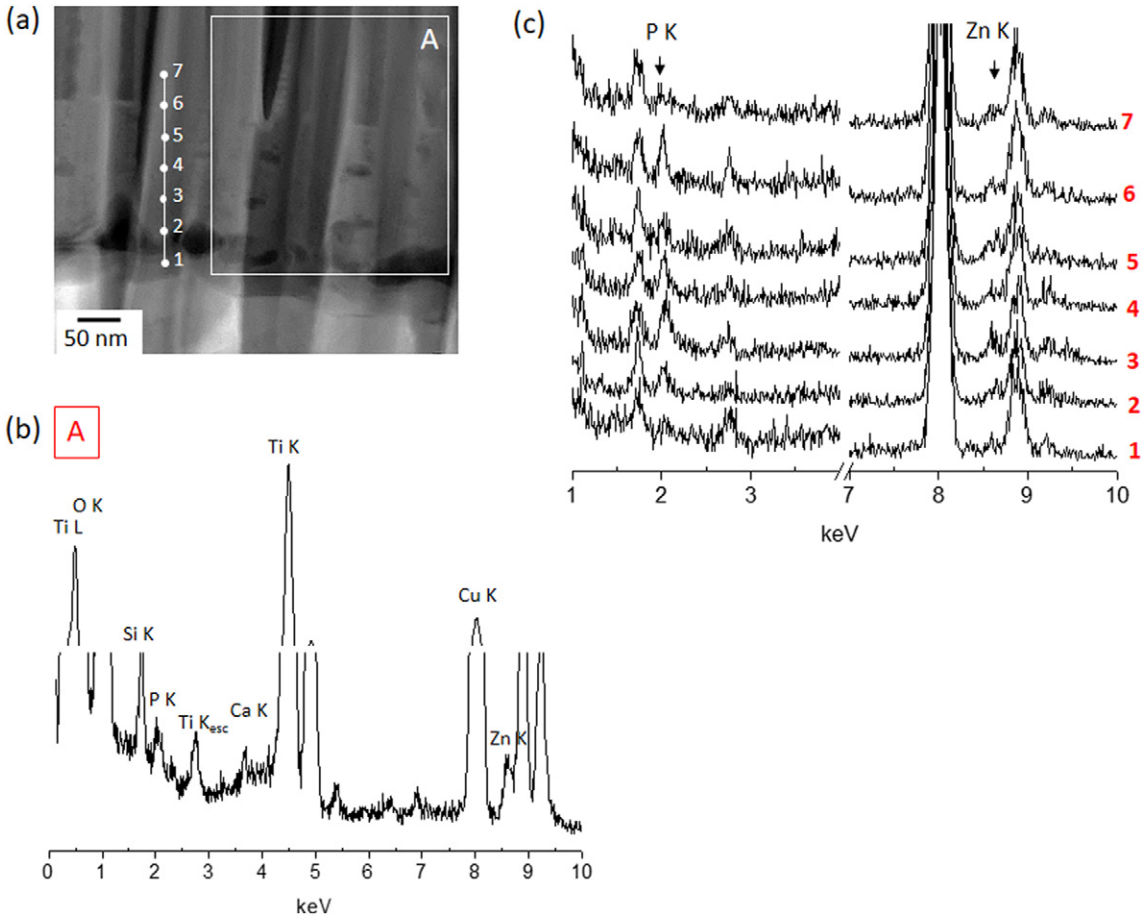

Fig. 10. STEM-EDS analyses in the interface region of NT-Ca/P/Zn film: (a) STEM-DF image showing the NT-Ca/P/Zn film interface, with the white insets indicating where the elemental analyses were performed; (b) STEM-EDS spectrum obtained from the region comprised by the inset white square A in (a); (c) line scan STEM-EDS analyses along the nano-thick oxide film formed by anodization, as indicated the white spots numbered in (a) from 1 to 7.

and Fig. 8c). From the STEM-EDS spectra in Fig. 4c and Fig. 5c it can be observed that Ti and O were detected, related with the presence of Ti oxide composing the nanotubes. The uniform distribution of Ti, O and F elements was also observed along the length of NT-Ca/P and NT-Ca/P/Zn films, through STEM-EDS elemental maps taken in the upper, middle and interface region of these films (Supplementary material). These results indicate that bio-functionalization processes have not influenced the composition of the nanotubes regarding its F content. Beyond other techniques have been used to modify the chemical properties of Ti, in particular, reverse polarization has been revealed as a versatile approach to develop bio-functional implant surfaces for biomedical applications [25,68–70].

4.2. Characterization of Ti/TiO_2 nanotubes interface

Beyond the wide range of studies reported in literature showing the promising features of TiO_2 nanotubes for the design of new implant systems, little knowledge still exists on their adhesion properties to the Ti substrate, and therefore on their ability to ensure an appropriate long term biomechanical stability. Recently, a few studies have shown that TiO_2 nanotubes are susceptible to peeling off from the underlying substrate, while rinsing with water or drying, because of the poor adhesion strength of TiO_2 nanotubes to Ti [37,46]. For this reason, the interfacial features of the TiO_2 nanotubular films produced by two-step anodization of Ti were investigated. After the second anodization step for TiO_2 nanotube synthesis, the presence of a non-continuous interface was found between the nanotubular film and the Ti substrate, as shown in Fig. 6. This interface is characterized by a hollow space extended over the film width.

Aiming to understand the mechanisms underlying the TiO_2 nanotube film detachment, researchers have recently made interesting findings. Different mechanisms have been proposed for nanotube detachment, namely the water assisted dissolution of the fluoride-rich layer existing beneath the nanotubes [37,46]. It has been generally accepted that a layer enriched with fluoride is formed at the oxide/metal interface during anodization. This layer can be ascribed to the twice fast migration rate of F^- compared to O^{2-} ions, resulting in a fluoride rich layer which has a thickness of a few tens of nanometers [37,61]. The existence of this fluoride rich layer was already proved by XPS sputter profiles taken from the tube bottom side of the tubes [71]. In accordance with Miraghaei et al. [46], TiO_2 nanotubes are detached from the substrate after immersion in aqueous solutions due to dissolution of TiF_4 layer existing between the tubes and Ti. Therefore, the existence of an interfacial hollow space after anodization of Ti might be related to water assisted dissolution of a fluoride-rich layer formed underneath the nanotubes. The hollow space existing between Ti substrate and TiO_2 nanotubes bottom is of a few tens of nanometers (Fig. 6b), similar to the thickness reported for the fluoride-rich layer [61]. Notwithstanding, as reported by Zhao et al. [47], the existence of this non-continuous interface might be also related to a hydrogen-assisted crack mechanism.

Researchers have recently made some efforts to improve the adhesion between TiO_2 nanotubes and Ti substrate. Zhao et al. [47] reported a novel method to control the detachment of TiO_2 nanotubes by their post-treatment in solvents with different polarities. The beneficial effect of anodization of TiO_2 nanotubes has been reported by Miraghaei et al. [46] and Yu et al. [37] due to the formation of a new barrier layer beneath them. Recently, annealing was also a method used by Roguska et al. [72] to stabilize the interfacial region between Ti substrate and

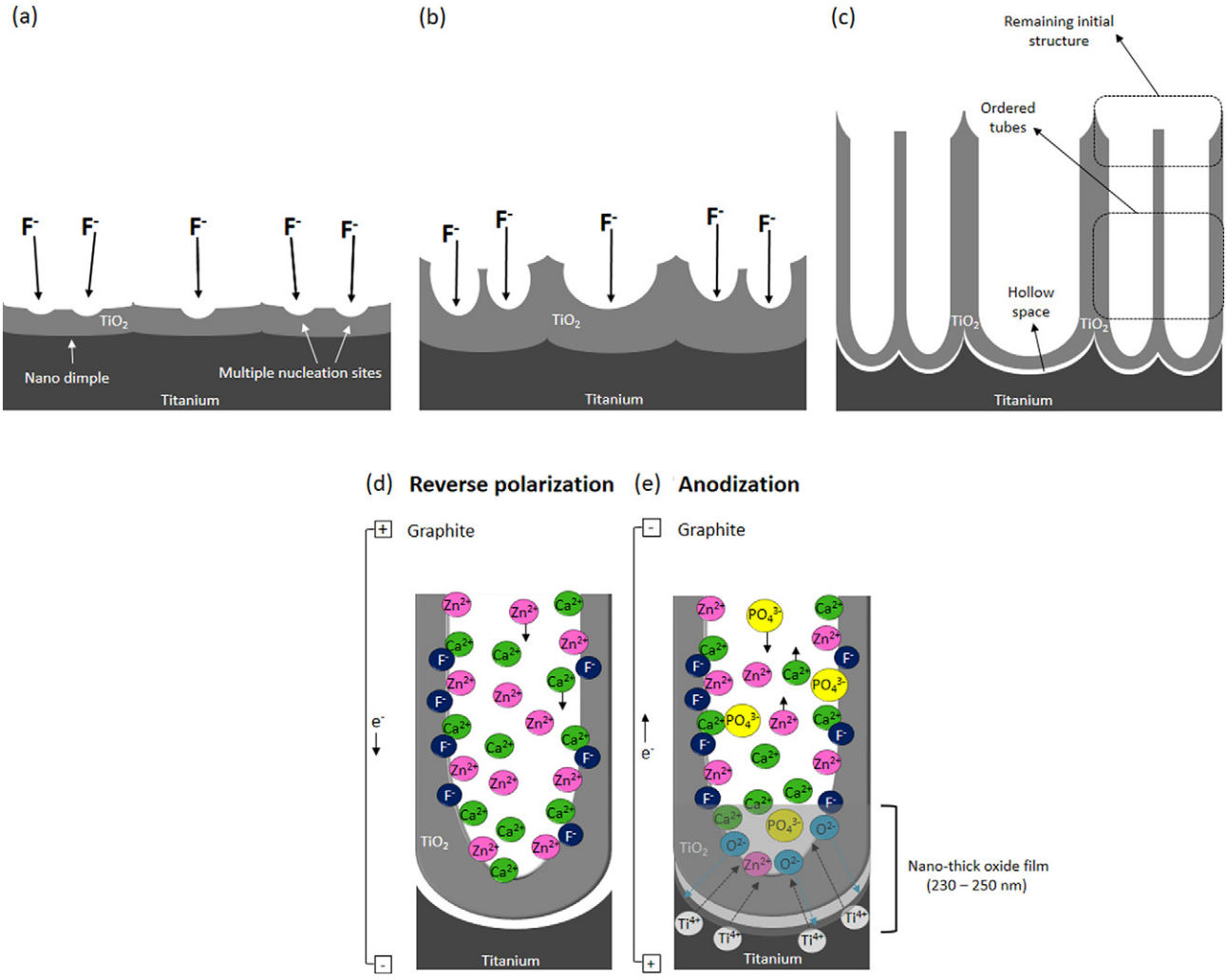

Fig. 11. Illustration of the different growth stages of TiO_2 nanotubes from nano-patterned Ti substrates. In (a) it is depicted the first stage during which the local chemical dissolution of the growing anodic oxide film by F^- ions takes place, with the nano-imprinted dimples acting as single or multiple nucleation sites; in (b) is shown a second stage in which the pronounced dissolution takes place at the bottom of the pores, where the electric filed is stronger; finally in (c) is depicted a later stage achieved after a long period of anodization (i.e. 30 min), after which the initial structure remains in the top region of the film while ordered tubes are underneath. The schematic illustration of the bio-functionalization mechanisms of TiO_2 nanotubes by reverse polarization and anodization are shown in (d) and (e), respectively. During anodization, Ti^{4+} ions are generated as a consequence of the polarization of Ti and they migrate across the hollow space and the bottom part of the tubes reacting with O^{2-} ions, leading to the formation of a Ti oxide film with thickness comprised between 230 and 250 nm.

TiO_2 nanotubes. However, beyond the potential of the previously reported methodologies to improve the adhesion strength of TiO_2 nanotubes, the morphological and chemical characterization of the Ti/TiO_2 interface is still missing. The creation of new knowledge on this field is of upmost relevance since it will provide a better comprehension of the adhesion phenomenon, before and after functionalization treatments, therefore providing new insights for further improvements.

4.3. Understanding the bio-functionalization mechanisms of TiO_2 nanotubes by reverse polarization and anodization

After bio-functionalization of TiO_2 nanotubes it is observed an interface with different features when compared to conventional TiO_2 nanotubes, as a consequence of the formation of a nano-thick oxide film at the interface region of NT-Ca/P and NT-Ca/P/Zn films, which presents a nanoporous morphology (Fig. 7). To explain this observation, current vs. time evolution recorded during bio-functionalization processes in the Ca/P and Ca/P/Zn-based electrolytes were considered (Fig. 8b and c). During anodization processes, three main stages can be identified. Firstly, once 100 V is applied, there is an increase in current values to its limiting value of 2.5 A (0.5 A/cm^2, first stage), followed by a period during which the current drops very quickly to values of 9.2 mA (2 mA/cm^2, second stage), a stage that is kept constant until the end of the anodization process (third stage). This is the typical current vs. time evolution characteristic of the growth behavior of a compact oxide film on Ti by anodization in a fluoride free electrolyte [54], whose growth mechanisms have been previously studied [73–75]. A similar behavior was reported by Oliveira et al. [51] during anodic oxidation of Ti in an electrolyte with composition similar to the one used in this study. The authors explained that the first stage of the graph (with limiting current of 2.5 A), is related to the time during which a high current contributes to the fast growth of the oxide film. As the oxide becomes thicker, its resistivity increases resulting in the decrease of the current to lower values, most likely due to the high resistivity of the newly oxide film formed that is kept constant with time. Dyer and Leach [73] also proposed that the non-linear voltage vs. time behavior observed during the galvanostatic anodic film growth on Ti, might be explained by changes in the ionic conductivity of the oxide. The behavior observed in Fig. 8b and c explains the nano-thick oxide film formation observed in Fig. 7, independently of the electrolyte composition. A longer duration for the first stage was achieved for anodization in the Ca/P/Zn electrolyte, probably related with its higher conductivity (Fig. 8c). Oliveira et al. [51] reported that as higher this period, higher the total charge in the system is. The authors pointed out that

theoretically, this would influence the total amount of oxide grown during the process, with effects on the measured thickness and compactness of the film. This may be related with the more pronounced points of contact existing between the Ti substrate and NT-Ca/P/Zn film, when compared to the ones exiting at NT-Ca/P film interface, as observed in Fig. 7a and Fig. 7b. Nonetheless, no significant differences were found in the thickness of the newly formed interfacial films, as in both cases, thickness ranges between 230 and 250 nm.

The study of the chemical composition of the nano-thick films formed by anodization showed that these are composed of O and Ti, including in the inter pore-areas, evidencing the growth of a Ti oxide (Fig. 7c, Fig. 7d and Supplementary material). Furthermore, the lighter contrast at the nano-thick oxide film region observed in STEM-DF images (Fig. 7), evidences the presence of a film with a higher density compared to the one in a darker area. The existence of the bioactive elements (i.e. Ca, P and Zn) at the interface region (Fig. 9 and Fig. 10) shows that the electrolyte penetrated along the film length during functionalization processes. Line scan STEM-EDS analyses along and across the uppermost region of the nano-thick film formed in NT-Ca/P interface (Fig. 9a), shows that Ca was not homogeneously distributed along the film (Fig. 9c) and interestingly, appeared to be entrapped on it (Fig. 9d). Ca entrapment at the interface is an additional indicator that the oxide film was formed during bio-functionalization processes. Line scan STEM-EDS analysis along NT-Ca/P/Zn interface evidenced a non-uniform distribution of Zn and P across the nano-thick oxide film formed. Beyond Ca has been detected in this interface (Fig. 10b), its presence was not identified along the line scan analyses, and this might be related with its non-uniform distribution along the film length, as discussed previously.

As previously reported by Chen et al. [25], by cathodic polarization of TiO_2 nanotubes in a Ca- and P-containing electrolyte, nanoscale calcium phosphate was successfully deposited on the inner and outer walls of the nanotubes. Furthermore, Huang et al. [76] observed the deposition of a hydroxyapatite coating composed of Cu and Zn on Ti surfaces, which was synthesized by electrodeposition method in an electrolyte containing Ca, Cu, Zn and P. In accordance with these previous studies, during reverse polarization, it is believed that positively charged ions in solution, namely Ca^{2+} and Zn^{2+} ions, are directed towards TiO_2 nanotube surface and penetrate the nanotubes towards its bottom part, as schematically illustrated in Fig. 11d. It is believed that during this stage, part of the Ca^{2+} and Zn^{2+} ions are adsorbed to TiO_2, and possibly Ca^{2+} ions react with F^- ions. It is noteworthy that F^- ions are present on TiO_2 nanotube wall as a result of the nanotube synthesis process. As soon as the anodization process starts, it is expected that an inversion in the electrode polarity leads to an inversion on the ions movement: those positively charged still remaining in solution, such as Ca^{2+} and Zn^{2+}, tend to move away the bottom part of the film and, on the other hand, negatively charged ions such as phosphate (PO_4^{3-}), are directed towards the interface as illustrated in Fig. 11e. Simultaneously, it is expected that Ti^{4+} ions are generated at Ti surface, and under the action of the electric filed, migrate through the hollow interface and the bottom part of the tubes towards the oxide-electrolyte interface, reacting with O^{2-} ions moving in opposite direction and leading to the formation of the Ti oxide film [54,66,77,78]. As explained in previous studies, anodization induces to the field-enhanced oxidation of Ti accompanied by the release of Ti^{4+} ions, which react with O^{2-} ions created by field-assisted deprotonation of H_2O or OH^- ions present in the electrolyte, a reaction that takes place at the oxide-electrolyte interface [54,66]. Khalil and Leach [74] also explained that the oxide growth under the influence of the electric field involves the diffusion of both metal and oxygen, and is dependent on the relative movement of the two species through the oxide. A possible mechanism for Ca entrapment at the interface region can be ascribed to the growing of the oxide film during anodization and the simultaneous movement of positively charged Ca^{2+} ions in direction to the uppermost part of the nanotubes.

In our previous work [48], TiO_2 nanotubes displayed a significantly lower passive current in artificial saliva after bio-functionalization treatments, independently of reverse polarization step. From the findings achieved in this investigation, the formation of a nano-thick oxide film as a consequence of anodization might be the reason for the significant improvement on the electrochemical behavior of nanotubular films. These results indicate that the nano-thick oxide film display the ability to protect the Ti substrate against corrosion, thus guaranteeing good prospects for their application for osseointegrated implants.

The formation of an oxide film as a consequence of anodization in an aqueous electrolyte might influence the adhesion of the film to Ti substrate. This is an issue of main importance and therefore further adhesion tests should be conducted. Furthermore, the investigation of the mechanical properties of the bio-functionalized TiO_2 nanotubes would be also of valuable interest. The mechanical properties of the films dictate their ability to withstand to mechanical stress, and thus to resist to degradation. The investigation of the degradation behavior of TiO_2 nanotubular samples before and after bio-functionalization, should be addressed under the simultaneous action of wear and corrosion (tribocorrosion), aiming to simulate the harsh and real conditions that osseointegrated implants are submitted to. Lastly, but not the least, a deepest investigation on the biological responses to these bio-functionalized TiO_2 nanotubes is of upmost importance. More specific biological assays must be accomplished to ensure that the surface features of these structures do not compromise the cellular functions.

5. Conclusions

Bioactive elements of Zn, Ca, and P were successfully incorporated in TiO_2 nanotubular structures through reverse polarization and anodization processes. Cross-sectioned bio-functionalized nanotubular films were characterized regarding morphology and chemistry with a special focus given to Ti/TiO_2 nanotubes interface. Hereafter the main outcomes of this research are highlighted:

- The incorporation of Ca, P and Zn elements in TiO_2 nanotubes was successfully achieved by reverse polarization and anodization processes, with the bioactive elements uniformly distributed along the topmost regions of the films as well along their length.
- Bio-functionalization treatments do not compromise the bone-inspired morphology of TiO_2 nanotubes, neither their high self-ordering nor integrity.
- The anodization of TiO_2 nanotubes in aqueous electrolytes induces the growth of a nano-thick protective oxide film (230–250 nm) at the Ti/TiO_2 nanotube interface region, which appears to improve the interfacial features, suggesting a better adhesion property. This interfacial nano-thick oxide film is constituted by Ca, P and Zn, however, these elements appeared to be non-uniformly distributed across the film length, with Ca found to be entrapped on its superficial region.

Reverse polarization arises as a fundamental step to provide biocompatibility to TiO_2 nanotubes while anodization promotes the growth of a nano-thick oxide film at the Ti/TiO_2 interface, enhancing the corrosion behavior of TiO_2 nanotubes. Additionally, the growth of the nano-thick oxide film improves the bonding strength of the nanotubular film to the Ti substrate, a critical factor determining the biomechanical stability of an implant, and so its long-term success. This work brings up a first insight on the bio-functionalization mechanisms of TiO_2 nanotubular films by reverse polarization and anodization processes. This novel methodology may inspire the emergence of novel surface treatment strategies seeking the long-term performance of metallic-modified implants.

Supplementary data to this article can be found online at http://dx.doi.org/10.1016/j.surfcoat.2017.05.073.

Acknowledgements

The authors would like to thank the Portuguese Foundation for Science and Technology for the doctoral grant (Ref. SFRH/BD/88517/2012) as well CNPq (Brazil - Ref. 490761/2013-5) and CAPES (Brazil - Ref. 99999.008666/2014-08) for the financial support. Also, the authors acknowledge all the support from LABNANO/CBPF (Brazilian Center for Research in Physics) for electron microscopy analyses. Tolou Shokuhfar is especially thankful to US National Science Foundation NSF-DMR CAREER award# 1564950 for providing partial financial support.

References

[1] M. Navarro, A. Michiardi, O. Castano, J. Planell, Biomaterials in orthopaedics, J. R. Soc. Interface 5 (2008) 1137–1158.
[2] S. Bauer, P. Schmuki, K. von der Mark, J. Park, Engineering biocompatible implant surfaces: part I: materials and surfaces, Prog. Mater. Sci. 58 (2013) 261–326.
[3] Y. Oshida, E.B. Tuna, O. Aktören, K. Gençay, Dental implant systems, Int. J. Mol. Sci. 11 (2010) 1580–1678.
[4] K.G. Neoh, X. Hu, D. Zheng, E.T. Kang, Balancing osteoblast functions and bacterial adhesion on functionalized titanium surfaces, Biomaterials 33 (2012) 2813–2822.
[5] P.A. Norowski, J.D. Bumgardner, Biomaterial and antibiotic strategies for peri-implantitis: a review, J. Biomed. Mater. Res. B Appl. Biomater. 88B (2009) 530–543.
[6] T.D. Taylor, Prosthodontic problems and limitations associated with osseointegration, J. Prosthet. Dent. 79 (1998) 74–78.
[7] J.A. Porter, J.A. Von Fraunhofer, Success or failure of dental implants? A literature review with treatment considerations, Gen. Dent. 53 (2004) 423–432 (quiz 433, 446).
[8] Y. Yu, G. Jin, Y. Xue, D. Wang, X. Liu, J. Sun, Multifunctions of Dual Zn/mg ion co-Implanted Titanium on Osteogenesis, Angiogenesis and Bacteria Inhibition for Dental Implants, Acta Biomaterialia, 2016.
[9] G. Subbiahdoss, R. Kuijer, D.W. Grijpma, H.C. van der Mei, H.J. Busscher, Microbial biofilm growth vs. tissue integration: "the race for the surface" experimentally studied, Acta Biomater. 5 (2009) 1399–1404.
[10] K. Gulati, M.S. Aw, D. Losic, Drug-eluting Ti wires with titania nanotube arrays for bone fixation and reduced bone infection, Nanoscale Res. Lett. 6 (2011) 571.
[11] S. Svensson, F. Suska, L. Emanuelsson, A. Palmquist, B. Norlindh, M. Trobos, H. Bäckros, L. Persson, G. Rydja, et al., Osseointegration of titanium with an antimicrobial nanostructured noble metal coating, Nanomedicine: Nanotechnology, Biology and Medicine 9 (2013) 1048–1056.
[12] W. Zhang, G. Wang, Y. Liu, X. Zhao, D. Zou, C. Zhu, Y. Jin, Q. Huang, J. Sun, et al., The synergistic effect of hierarchical micro/nano-topography and bioactive ions for enhanced osseointegration, Biomaterials 34 (2013) 3184–3195.
[13] H. Yazici, H. Fong, B. Wilson, E. Oren, F. Amos, H. Zhang, J. Evans, M. Snead, M. Sarikaya, et al., Biological response on a titanium implant-grade surface functionalized with modular peptides, Acta Biomater. 9 (2013) 5341–5352.
[14] H.-L. Huang, Y.-Y. Chang, J.-C. Weng, Y.-C. Chen, C.-H. Lai, T.-M. Shieh, Anti-bacterial performance of zirconia coatings on titanium implants, Thin Solid Films 528 (2013) 151–156.
[15] G. Jin, H. Qin, H. Cao, Y. Qiao, Y. Zhao, X. Peng, X. Zhang, X. Liu, P.K. Chu, Zn/Ag micro-galvanic couples formed on titanium and osseointegration effects in the presence of *S. aureus*, Biomaterials 65 (2015) 22–31.
[16] N. Swami, Z. Cui, L.S. Nair, Titania nanotubes: novel nanostructures for improved osseointegration, J. Heat Transf. 133 (2011), 034002.
[17] G. Balasundaram, T.J. Webster, Nanotechnology and biomaterials for orthopedic medical applications, Nanomedicine 1 (2006) 169–176.
[18] C.R. Friedrich, M. Kolati, T. Moser, C. Sukotjo, T. Shokuhfar, Survivability of TiO_2 nanotubes on the surface of bone screws, Surface Innovations 2 (2014) 60–68.
[19] S. Bhosle, S. Patel, M.M. Taheril, C. Sukotjo, T. Shokuhfar, Electrochemical anodization of Ti-15Zr implant: effect of different voltage and time, Surface Innovations (2017) 1–26.
[20] A. Robin, M.B. de Almeida Ribeiro, J.L. Rosa, R.Z. Nakazato, M.B. Silva, Formation of TiO_2 nanotube layer by anodization of titanium in ethylene glycol-H_2O electrolyte, Journal of Surface Engineered Materials and Advanced Technology 2014 (2014).
[21] M. Kulkarni, A. Mazare, J. Park, E. Gongadze, M.S. Killian, S. Kralj, K. von der Mark, A. Iglič, P. Schmuki, Protein interactions with layers of TiO_2 nanotube and nanopore arrays: morphology and surface charge influence, Acta Biomater. (2016) 357–366.
[22] A. Tian, X. Qin, A. Wu, H. Zhang, Q. Xu, D. Xing, H. Yang, B. Qiu, X. Xue, et al., Nanoscale TiO_2 nanotubes govern the biological behavior of human glioma and osteosarcoma cells, Int. J. Nanomedicine 10 (2015) 2423–2439.
[23] A. Hamlekhan, A. Butt, S. Patel, D. Royhman, C. Takoudis, C. Sukotjo, J. Yuan, G. Jursich, M.T. Mathew, et al., Fabrication of anti-aging TiO_2 nanotubes on biomedical Ti alloys, PLoS One 9 (2014), e96213.
[24] L. Lv, Y. Liu, P. Zhang, X. Zhang, J. Liu, T. Chen, P. Su, H. Li, Y. Zhou, The nanoscale geometry of TiO2 nanotubes influences the osteogenic differentiation of human adipose-derived stem cells by modulating H3K4 trimethylation, Biomaterials 39 (2015) 193–205.
[25] J. Chen, Z. Zhang, J. Ouyang, X. Chen, Z. Xu, X. Sun, Bioactivity and osteogenic cell response of TiO_2 nanotubes coupled with nanoscale calcium phosphate via ultrasonification-assisted electrochemical deposition, Appl. Surf. Sci. 305 (2014) 24–32.
[26] A. Roguska, M. Pisarek, M. Andrzejczuk, M. Dolata, M. Lewandowska, M. Janik-Czachor, Characterization of a calcium phosphate-TiO_2 nanotube composite layer for biomedical applications, Mater. Sci. Eng. C 31 (2011) 906–914.
[27] C.J. Frandsen, K.S. Brammer, K. Noh, G. Johnston, S. Jin, Tantalum coating on TiO_2 nanotubes induces superior rate of matrix mineralization and osteofunctionality in human osteoblasts, Mater. Sci. Eng. C 37 (2014) 332–341.
[28] T. Shokuhfar, A. Hamlekhan, J.-Y. Chang, C.K. Choi, C. Sukotjo, C. Friedrich, Biophysical evaluation of cells on nanotubular surfaces: the effects of atomic ordering and chemistry, Int. J. Nanomedicine 9 (2014) 3737.
[29] A. Mazare, G. Totea, C. Burnei, P. Schmuki, I. Demetrescu, D. Ionita, Corrosion, antibacterial activity and haemocompatibility of TiO_2 nanotubes as a function of their annealing temperature, Corros. Sci. 103 (2016) 215–222.
[30] Z. Guo, C. Chen, Q. Gao, Y. Li, L. Zhang, Fabrication of silver-incorporated TiO_2 nanotubes and evaluation on its antibacterial activity, Mater. Lett. 137 (2014) 464–467.
[31] H. Li, Q. Cui, B. Feng, J. Wang, X. Lu, J. Weng, Antibacterial activity of TiO_2 nanotubes: influence of crystal phase, morphology and Ag deposition, Appl. Surf. Sci. 284 (2013) 179–183.
[32] Y. Zhao, Q. Xing, J. Janjanam, K. He, F. Long, K.-B. Low, A. Tiwari, F. Zhao, R. Shahbazian-Yassar, et al., Facile electrochemical synthesis of antimicrobial TiO_2 nanotube arrays, Int. J. Nanomedicine 9 (2014) 5177.
[33] H. Zhang, Y. Sun, A. Tian, X.X. Xue, L. Wang, A. Alquhali, X. Bai, Improved antibacterial activity and biocompatibility on vancomycin-loaded TiO_2 nanotubes: in vivo and in vitro studies, Int. J. Nanomedicine 8 (2013) 4379.
[34] K. Gulati, S. Ramakrishnan, M.S. Aw, G.J. Atkins, D.M. Findlay, D. Losic, Biocompatible polymer coating of titania nanotube arrays for improved drug elution and osteoblast adhesion, Acta Biomater. 8 (2012) 449–456.
[35] T. Shokuhfar, S. Sinha-Ray, C. Sukotjo, A.L. Yarin, Intercalation of anti-inflammatory drug molecules within TiO_2 nanotubes, RSC Adv. 3 (2013) 17380–17386.
[36] A. Hamlekhan, S. Sinha-Ray, C. Takoudis, M.T. Mathew, C. Sukotjo, A.L. Yarin, T. Shokuhfar, Fabrication of drug eluting implants: study of drug release mechanism from titanium dioxide nanotubes, J. Phys. D. Appl. Phys. 48 (2015) 275401.
[37] D. Yu, X. Zhu, Z. Xu, X. Zhong, Q. Gui, Y. Song, S. Zhang, X. Chen, D. Li, Facile method to enhance the adhesion of TiO_2 nanotube arrays to Ti substrate, ACS Appl. Mater. Interfaces 6 (2014) 8001–8005.
[38] E. Mohseni, E. Zalnezhad, A. Bushroa, Comparative investigation on the adhesion of hydroxyapatite coating on Ti–6Al–4V implant: a review paper, Int. J. Adhes. Adhes. 48 (2014) 238–257.
[39] F. Velard, J. Braux, J. Amedee, P. Laquerriere, Inflammatory cell response to calcium phosphate biomaterial particles: an overview, Acta Biomater. 9 (2013) 4956–4963.
[40] A.R. Ribeiro, S. Gemini-Piperni, R. Travassos, L. Lemgruber, R. C. Silva, A.L. Rossi, M. Farina, K. Anselme, T. Shokuhfar, et al., Trojan-like internalization of anatase titanium dioxide nanoparticles by human osteoblast cells, Sci. Rep. 6 (2016) 23615.
[41] D. Olmedo, M. Paparella, D. Brandizzi, R. Cabrini, Reactive lesions of peri-implant mucosa associated with titanium dental implants: a report of 2 cases, Int. J. Oral Maxillofac. Surg. 39 (2010) 503–507.
[42] S.B. Goodman, T. Ma, R. Chiu, R. Ramachandran, R.L. Smith, Effects of orthopaedic wear particles on osteoprogenitor cells, Biomaterials 27 (2006) 6096–6101.
[43] L. Rocha, F. Oliveira, H. Cruz, C. Sukotjo, M. Mathew, Bio-tribocorrosion in biomaterials and medical implants, Bio-Tribocorrosion In Dental Applications, Elsevier Inc 2013, pp. 223–249.
[44] S. Alves, R. Bayón, A. Igartua, V. Saénz de Viteri, L. Rocha, Tribocorrosion behaviour of anodic titanium oxide films produced by plasma electrolytic oxidation for dental implants, Lubr. Sci. 26 (2014) 500–513.
[45] S. Alves, R. Bayón, V.S. de Viteri, M. Garcia, A. Igartua, M. Fernandes, L. Rocha, Tribocorrosion behavior of calcium-and phosphorous-enriched titanium oxide films and study of osteoblast interactions for dental implants, Journal of Bio-and Tribo-Corrosion 1 (2015) 1–21.
[46] S. Miraghaei, F. Ashrafizadeh, K. Raeissi, M. Santamaria, F. Di Quarto, An electrochemical investigation on the adhesion of As-formed anodic TiO2 nanotubes grown in organic solvents, Electrochem. Solid-State Lett. 14 (2011) K8–K11.
[47] M. Zhao, J. Li, Y. Li, J. Wang, Y. Zuo, J. Jiang, H. Wang, Gradient Control of the Adhesive Force between Ti/TiO2 Nanotubular Arrays Fabricated by Anodization, Scientific Reports 4, 2014.
[48] S.A. Alves, S.B. Patel, C. Sukotjo, M.T. Mathew, P.N. Filho, J.-P. Celis, L.A. Rocha, T. Shokuhfar, Synthesis of calcium-phosphorous doped TiO2 nanotubes by anodization and reverse polarization: a promising strategy for an efficient biofunctional implant surface, Appl. Surf. Sci. 399 (2017) 682–701.
[49] S.A. Alves, A.L. Rossi, A.R. Ribeiro, F. Toptan, A.M. Pinto, J.-P. Celis, T. Shokuhfar, L.A. Rocha, Tribo-electrochemical behavior of bio-functionalized TiO2 nanotubes in artificial saliva: understanding of degradation mechanisms, Wear 384–385 (2017) 28–42.
[50] A.R. Ribeiro, F. Oliveira, L.C. Boldrini, P.E. Leite, P. Falagan-Lotsch, A.B.R. Linhares, W.F. Zambuzzi, B. Fragneaud, A.P.C. Campos, et al., Micro-arc oxidation as a tool to develop multifunctional calcium-rich surfaces for dental implant applications, Mater. Sci. Eng. C 54 (2015) 196–206.
[51] F.G. Oliveira, A.R. Ribeiro, G. Perez, B.S. Archanjo, C.P. Gouvea, J.R. Araújo, A.P. Campos, A. Kuznetsov, C.M. Almeida, et al., Understanding growth mechanisms and tribocorrosion behaviour of porous TiO_2 anodic films containing calcium, phosphorous and magnesium, Appl. Surf. Sci. 341 (2015) 1–12.
[52] A.C. Alves, F. Oliveira, F. Wenger, P. Ponthiaux, J.-P. Celis, L.A. Rocha, Tribocorrosion behaviour of anodic treated titanium surfaces intended for dental implants, J. Phys. D. Appl. Phys. 46 (2013) 404001.
[53] D.B. Williams, C.B. Carter, Transmission Electron Microscopy: Springer US, 2009.
[54] P. Roy, S. Berger, P. Schmuki, TiO_2 nanotubes: synthesis and applications, Angew. Chem. Int. Ed. 50 (2011) 2904–2939.
[55] S. Patel, G.F. Solitro, C. Sukotjo, C. Takoudis, M.T. Mathew, F. Amirouche, T. Shokuhfar, Nanotopography and surface stress analysis of Ti6Al4V bioimplant: an alternative design for stability, JOM 67 (2015) 2518–2533.

[56] G. Ali, C. Chen, S.H. Yoo, J.M. Kum, S.O. Cho, Fabrication of complete titania nanoporous structures via electrochemical anodization of Ti, Nanoscale Res. Lett. 6 (2011) 1–10.
[57] X. Yuan, M. Zheng, L. Ma, W. Shen, High-speed growth of TiO_2 nanotube arrays with gradient pore diameter and ultrathin tube wall under high-field anodization, Nanotechnology 21 (2010) 405302.
[58] Z. Su, W. Zhou, Formation, morphology control and applications of anodic TiO_2 nanotube arrays, J. Mater. Chem. 21 (2011) 8955–8970.
[59] J. Macak, H. Hildebrand, U. Marten-Jahns, P. Schmuki, Mechanistic aspects and growth of large diameter self-organized TiO_2 nanotubes, J. Electroanal. Chem. 621 (2008) 254–266.
[60] H. Hu, W. Zhang, Y. Qiao, X. Jiang, X. Liu, C. Ding, Antibacterial activity and increased bone marrow stem cell functions of Zn-incorporated TiO_2 coatings on titanium, Acta Biomater. 8 (2012) 904–915.
[61] S. Berger, S.P. Albu, F. Schmidt-Stein, H. Hildebrand, P. Schmuki, J.S. Hammond, D.F. Paul, S. Reichlmaier, The origin for tubular growth of TiO_2 nanotubes: a fluoride rich layer between tube-walls, Surf. Sci. 605 (2011) L57–L60.
[62] T. Ohtsuka, M. Masuda, N. Sato, Cathodic reduction of anodic oxide films formed on titanium, J. Electrochem. Soc. 134 (1987) 2406–2410.
[63] M. Vezvaie, J.J. Noël, Z. Tun, D.W. Shoesmith, Hydrogen absorption into titanium under cathodic polarization: an in-situ neutron reflectometry and EIS study, J. Electrochem. Soc. 160 (2013) C414–C422.
[64] R. Torresi, O. Camara, C. De Pauli, Influence of the hydrogen evolution reaction on the anodic titanium oxide film properties, Electrochim. Acta 32 (1987) 1357–1363.
[65] E. Peláez Abellán, L. Rocha-Souza, A.C. Guastaldi, Cathodic behaviour of anodized titanium in simulated physiological, Lat. Am. Appl. Res. 41 (2011) 199–203.
[66] B.M. Rao, A. Torabi, O.K. Varghese, Anodically grown functional oxide nanotubes and applications, MRS Communications 6 (2016) 375–396.
[67] D. Devilliers, M.T. Dinh, E. Mahé, D. Krulic, N. Larabi, N. Fatouros, Behaviour of titanium in sulphuric acid-application to DSAs, J. New Mater. Electrochem. Syst. 9 (2006) 221.
[68] A. Gao, R. Hang, X. Huang, L. Zhao, X. Zhang, L. Wang, B. Tang, S. Ma, P.K. Chu, The effects of titania nanotubes with embedded silver oxide nanoparticles on bacteria and osteoblasts, Biomaterials 35 (2014) 4223–4235.
[69] C. Xie, P. Li, Y. Liu, F. Luo, X. Xiao, Preparation of TiO_2 nanotubes/mesoporous calcium silicate composites with controllable drug release, Mater. Sci. Eng. C 67 (2016) 433–439.
[70] L. Zhao, H. Wang, K. Huo, L. Cui, W. Zhang, H. Ni, Y. Zhang, Z. Wu, P.K. Chu, Antibacterial nano-structured titania coating incorporated with silver nanoparticles, Biomaterials 32 (2011) 5706–5716.
[71] S.P. Albu, A. Ghicov, S. Aldabergenova, P. Drechsel, D. LeClere, G.E. Thompson, J.M. Macak, P. Schmuki, Formation of double-walled TiO_2 nanotubes and robust anatase membranes, Adv. Mater. 20 (2008) 4135–4139.
[72] A. Roguska, M. Pisarek, A. Belcarz, L. Marcon, M. Holdynski, M. Andrzejczuk, M. Janik-Czachor, Improvement of the bio-functional properties of TiO_2 nanotubes, Appl. Surf. Sci. (2016).
[73] C.K. Dyer, J.S.L. Leach, Breakdown and efficiency of anodic oxide growth on titanium, J. Electrochem. Soc. 125 (1978) 1032–1038.
[74] N. Khalil, J.S.L. Leach, The anodic oxidation of valve metals—I. Determination of ionic transport numbers by α-spectrometry, Electrochim. Acta 31 (1986) 1279–1285.
[75] D. Scharnweber, R. Beutner, S. Rößler, H. Worch, Electrochemical behavior of titanium-based materials–are there relations to biocompatibility? J. Mater. Sci. Mater. Med. 13 (2002) 1215–1220.
[76] Y. Huang, X. Zhang, H. Mao, T. Li, R. Zhao, Y. Yan, X. Pang, Osteoblastic cell responses and antibacterial efficacy of Cu/Zn co-substituted hydroxyapatite coatings on pure titanium using electrodeposition method, RSC Adv. 5 (2015) 17076–17086.
[77] D. Gong, C.A. Grimes, O.K. Varghese, W. Hu, R.S. Singh, Z. Chen, E.C. Dickey, Titanium oxide nanotube arrays prepared by anodic oxidation, J. Mater. Res. 16 (2001) 3331–3334.
[78] J.M. Macak, H. Tsuchiya, A. Ghicov, K. Yasuda, R. Hahn, S. Bauer, P. Schmuki, TiO_2 nanotubes: self-organized electrochemical formation, properties and applications, Curr. Opinion Solid State Mater. Sci. 11 (2007) 3–18.